



PREPARATION AND CHARACTERISATION OF ZnO THIN FILMS DEPOSITED BY RF SPUTTERING METHOD

¹Abdullahi, S., ¹Abdullahi, M. B., ^{*1}Abdullahi, B. and ²Wara, A. M.

¹Department of Physics, Usmanu Danfodiyo University, Sokoto, Nigeria

²Department of Science and Technology, Waziri Umaru Federal Polytechnic, Kebbi St, Nigeria

*Corresponding authors' email: bilyabdul@gmail.com

ABSTRACT

Zinc oxide (ZnO) thin films deposited on corning glass substrates at 100°C substrate temperature by radio frequency deposition were annealed the open air and microwave oven at 150°C. The influence of open-air annealing (OAA) and microwave annealing (MWA) were studied. The results obtained showed that MWA annealing can improve not only the crystal but also the optical properties of the ZnO thin films. A high transmittance is obtained in all the annealed samples (S₁, S₂, S₄ and S₅) demonstrating >90% at 650 nm wavelength. Reflectance in all the samples was < 29% with a minimum standing at 23.78% as recorded for sample S₅. The band gap for the annealed samples (S₁, S₂, S₄ and S₅) was determined at 3.26 eV, 3.32 eV, 3.29 eV and 3.34 eV respectively. Absorption coefficient stood at 0.0225 cm⁻¹, 0.0179 cm⁻¹, 0.0180 cm⁻¹, 0.0186 cm⁻¹ and 0.0181 cm⁻¹ for the as-deposited sample and the respectively. The optical and structural properties analysis showed that OAA and MWA annealing at suitable temperatures considered can significantly improve some properties of the ZnO thin films making the films suitable for applications in optoelectronics and photovoltaics.

Keywords: Zinc oxide, Microwave annealing (MWA), open-air annealing (OAA), RF Sputtering, XRD

INTRODUCTION

Transparent conducting oxides (TCOs) are a special class of materials that can simultaneously be both optically transparent and electrically conducting and, as such, are a critical component in almost all thin-film photovoltaic devices (Raghavendra and Bhat, 2017). TCOs are generally based on a limited class of metal oxide semiconductors such as In₂O₃, ZnO and SnO₂, which are transparent due to their large band gap and can also tolerate very high electronic doping concentrations to yield conductivities of 1000 S/cm or higher. TCOs consist of a group of materials that can be thought of as 'conjugate property materials' in which one property, such as conductivity, is strongly coupled to a second property, namely, such as the extinction coefficient. In this regard, it can be stated that materials like metals, that are highly conductive, will not normally transmit visible light, while highly transparent media like oxide glasses behave as insulators. Three oxides have emerged as commercially important transparent conductors (ITO): Indium Oxide, Tin Oxide, and Zinc Oxide.

Zinc oxide (ZnO) thin films have emerged as a promising material for various applications in electronics, optoelectronics, biomedical and sensing. The high conductivity and transparency of ZnO make it important for applications like transparent conducting oxides (TCO) and thin-film transistors (TFT) (Vyas, 2020). In addition, ZnO thin films can be easily prepared in the form of thin films, nanowires, nanorods, crystalline nanoparticles and flower-like structures (Laurenti and Cauda, 2018). ZnO is a direct band gap semiconductor of wurtzite structures and one of the most significant binary II-VI compounds. It is ideal for short-wavelength optoelectronic applications (Abdullahi et al., 2017). At room temperature, ZnO displays an effective radiative recombination rate and a direct bandgap of 3.3 to 3.37 eV. It operates in the UV to blue spectrum and is transparent to visible light thanks to its large exciton binding energy of 60 meV, which is 2.4 times higher than that of gallium nitride (GaN). This large exciton binding energy

opens the door for a strong near-band edge excitonic emission at room temperature and even higher (Senay et al., 2014; Zulkifli et al., 2015).

Zinc oxide thin films have been prepared by various deposition methods such as thermal oxidation (Rakesh and Vaidayan, 2009), Spin coating (Godbole et al., 2011, Chaitra et al., 2017), Vacuum Evaporation (Eya 2006) and RF sputtering (Viswanathan et al., 2016, Kumar et al., 2015, Shun-Fa and Li, 2013, Goncalves et al., 2016).

Among vacuum thin film deposition methods, the RF sputtering technique is widely used for electrically non-conductive target materials deposition. Compared to direct current (DC) sputtering, RF sputtering has several advantages such as compatibility with non-conductive materials which are not applicable for DC sputtering. It also has better film adhesion, reproducibility, and high deposition rate (Tchenka et al., 2021). RF sputtering creates more uniform films with better surface adhesion of target atoms and higher electron densities, even at low temperatures (Davidse and Maissel, 1993). RF sputtering is also most suitable for large-area substrates deposition (Shakoury et al., 2022). In this communication, we aim to present the preparation and characterization of ZnO thin films deposited by radio frequency sputtering method.

MATERIALS AND METHODS

Substrate cleaning and sample preparation:

Throughout the processing steps, great care was taken to ensure the cleanliness of the sample surfaces, as dirt and dust on the substrate prevented the material to be deposited from sufficiently bonding to the surface. Before the deposition, the substrates were kept in a dilute chemical detergent solution at 100°C in the ultrasonic bath for 10 minutes to remove oils and protein molecules and rinsed with double distilled water to remove possible left detergent contaminants. The substrates were then extracted from the bath and rinsed with distilled water and later dried with Nitrogen gas before being introduced into the sputtering chamber.

Thin film deposition

The ZnO thin films were deposited by RF sputtering using the Edwards RC 3000G (Auto 306) sputtering system. The vacuum pressure of the chamber was lowered to 8.6×10^{-6} Torr using a turbomolecular pump before introducing argon gas. The Working pressure was fixed at 1.6×10^3 Torr with an argon/oxygen flow rate of 1sccm a ratio 1:1. The distance between the target and substrate was maintained at 8.5 cm. Before deposition, the target was pre-sputtered for 10 minutes. The average thickness of the samples was 135 nm.

Annealing of the samples

In all, there were five (5) samples (S₁ to S₅) samples S₁ and S₂ were subjected to open air annealing (OAA) at 100°C and 150°C for 1 hour, samples S₄ and S₅ were annealed in a microwave oven (MWA) at 100°C and 150°C for 30 minutes, sample S₃ is the as-deposited sample

Characterization of samples

Structural properties of the ZnO films were studied using X-Pert pro X-ray diffraction system (XRD) equipped with a Cu source (wavelength $\lambda = 1.5418 \text{ \AA}$) in the range $2\theta = 20-80^\circ$, the scan speed is 0.8 degrees/minute at a scan step of 0.02. Transmittance, absorbance and reflectance spectra of the films in the region 180 to 1100 nm were recorded using AVANTES AVASPEC-2048 UV-VIS-NIR). Thin film thickness was measured using a Profilometer (STYLUS TAYLOR HOBSON MODEL). The electrical analysis of the samples was carried out using four-point probe.

Method of calculation

(i) The condition of diffraction is nothing but Bragg's Law and is given as:

$$2d \sin \theta = n\lambda \tag{1}$$

where **n** is the order of diffraction, **λ** is the wavelength of the X-ray, **d** is the spacing between consecutive parallel planes and **θ** is the glancing angle.

(ii) The average grain size (D) of the film (Abdullahi et al., 2017) can be calculated using Scherrer's formula.

$$D = \frac{0.9\lambda}{\beta \cos \theta} \tag{2}$$

where **λ** is the wavelength of the X-ray and **β** is the full width at half maximum (FWHM) intensity in radians.

(iii) The lattice parameter values for different crystallographic system can be calculated from the following equations (Abdullahi et al., 2017) using the (hkl) parameters and the interplanar spacing d.

Cubic system,

$$\frac{1}{d^2} = \frac{h^2 + k^2 + l^2}{a^2} \tag{3}$$

Hexagonal,

$$d^2(hkl) = \left[\frac{4(h^2 + k^2 + hk)}{3a^2} + \frac{l^2}{c^2} \right]^{-1} \tag{4}$$

(iv) The absorption coefficient **α** is related to the energy gap **E_g**, by Equation 5 (Pankaj., et al, 2020), where n=1 for direct band gap materials and n=2 for indirect band gap materials.

$$\alpha h = [hf - E_g]^{n/2} \tag{5}$$

For a direct gap material therefore the above Equation (5) becomes Expression (6).

$$E_g = hf - (\alpha hf)^2 \tag{6}$$

(v) The band gap energy **E_g** of film can be estimated by plotting **(αhf)²** versus **hf**.

Extrapolation of the linear portion of **(αhf)²** versus **(hf)** curve to intercept the horizontal photon energy axis will yield the direct band gap.

(vi) Some of the equations for calculating optical constants according to (Al-ofi et al., 2012) are;

The refractive index;

$$n = \frac{1+R^{0.5}}{1-R^{0.5}} \tag{7}$$

where **n** is the refractive index and **R** is the reflectance of the ZnO films.

Extinction coefficient (k):

$$k = \alpha\gamma/4\pi \tag{8}$$

where **k** is the extinction coefficient, **α** the absorption coefficient and **γ** is the wavelength (Al-ofin et al., 2012).

Dielectric constant (**ε**):

$$\epsilon = n^2 - k^2 \tag{9}$$

where **n** is the refractive index, and **k** is the extinction coefficient.

RESULTS AND DISCUSSION

Structural properties

Figure 1 displays the XRD pattern of samples annealed the open-air, annealed in microwave oven and the as-deposited sample (S₁ to S₅) respectively. It can be seen that four of the samples have a high-intensity peak at the (002) plane of reflection according to ICDD Card Number: 96-210-7060. The XRD spectra have shown no secondary phase. The absence of a secondary phase indicates that the sample has a C-axis orientation (Yilmaz., 2014). A decrease in the intensity of a peak can be related to the substitution of a lattice site by an ion-lowering radius. The interplanar spacing (d) decreases and the peak position changes accordingly. The lattice constants they have been calculated by Equation 4 above. It has been observed that the (002) diffraction peak intensity increases with an increase in annealing temperature for both Open Air Annealing (OAA) and Microwave Oven (MWA). This shows that annealing can lead to enhancement in the crystallinity of ZnO films. This enhancement may be related to the increase of atomic mobility and surface diffusion of the adsorbed species.

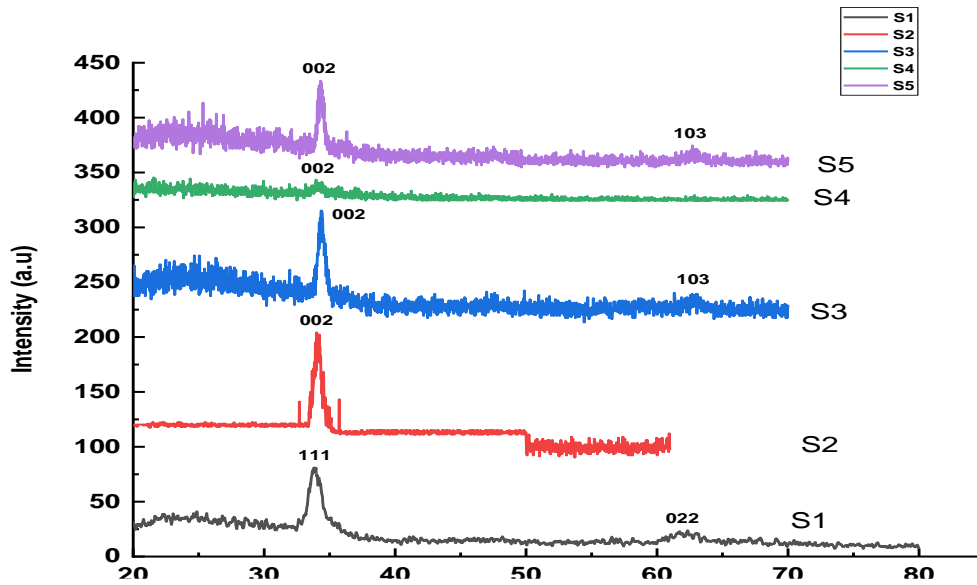


Figure 1. XRD patterns of the as-deposited sample (s₃) and samples annealed at 100°C for both OAA (s₁ and s₂) and MWA (s₄ and s₅).

The influence of annealing in the open air and microwave oven on the structural properties of ZnO thin films is presented in Table 1.

Table 1: Annealing condition, Diffraction angle, FWHM, Grain size, and Stress on ZnO Thin films

Annealing condition	As-deposited	OAA 100°C	OAA 150°C	MWA 100°C	MWA 150°C
2θ (deg.)	34.32	34.39	34.36	34.45	34.48
FWHM (002)	0.405	0.358	0.258	0.365	0.311
Grain size (nm)	21	24	26	23	28
Stress (GPa)	-1.374	-0.156	0.288	-0.867	1.126

The variation observed in the (002) peak position indicates the existence of residual stress between the ZnO film and the glass substrate, which is the combined effect of thermal stress and intrinsic stress. Because the thermal expansion coefficient of ZnO film is bigger than that of the glass substrate, there is a tensile stress in the ZnO films as the substrate cools down from high temperature to room temperature (Abdullahi et al., 2017), it has shown that the intrinsic stress of the as-deposited

ZnO films is compressive. The (002) positions of the as-deposited sample, samples annealed at 100°C and 150°C in open air, MWA100°C and MWA150°C are located at $2\theta = 34.32^\circ$, $2\theta = 34.39^\circ$, $2\theta = 34.36^\circ$, $2\theta = 34.45^\circ$ and $2\theta = 34.48^\circ$ as shown in Figure 2. The shift of the (002) position indicates both OAA and MWA reduce the residual stress. As the previous reports have shown (Kang et al., 2004), the (002) peak position increases with the annealing temperature.

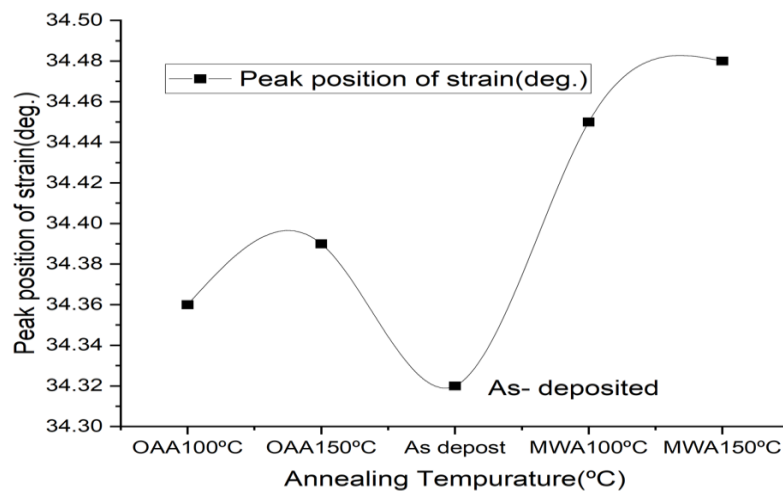


Figure 2: Peak position, Versus annealing temperature for ZnO thin films.

The estimated stress in ZnO films is displayed in Table (2) above and plotted in Figure 2. The residual stress of the as-deposited ZnO film is compressive, because there is a tensile stress in the ZnO films as the substrate cools down from high temperature to room temperature. By OAA at 100°C and MWA at 100°C, the residual stress of the ZnO films was relaxed. While increasing the MWA temperature to 150°C, the tensile stress becomes stronger than the compressive stress and changes the direction of stress. Comparing with OAA 150°C (Moreh et al., 2014) and the MWA shows a more

effective stress relaxation than OAA at the lower temperature. The energy transmission of MWA is produced by energy loss mechanisms of the electric vector, the microwave heating is volumetric, while that of OAA are conduction and convection process. The absorption of microwave power by solid materials is generally governed by their magnetic, dielectric, and conductive properties. Microwave oven heating occurs in thin films as a result of interfacial (space charge) and reorientation polarization.

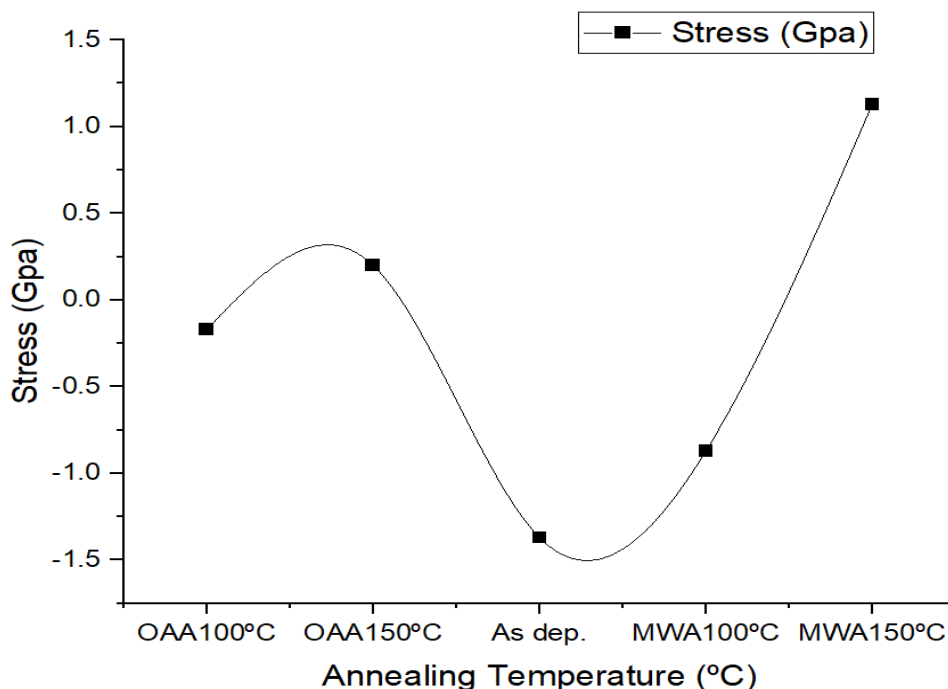


Figure 3: The stress is estimated from the (002) diffraction peak of XRD for ZnO films.

Assuming a homogeneous strain across the ZnO films, the average grain size can be estimated using Equation 2 from the full-width at half maximum (FWHM) of the (002) peak (Abdullahi et al., 2014). The calculated grain size is listed in

Table (1) and plotted in Figure 4. It is reasonable to say that MWA with a lower temperature (150°C) has better structure improvement than OAA (150°C).

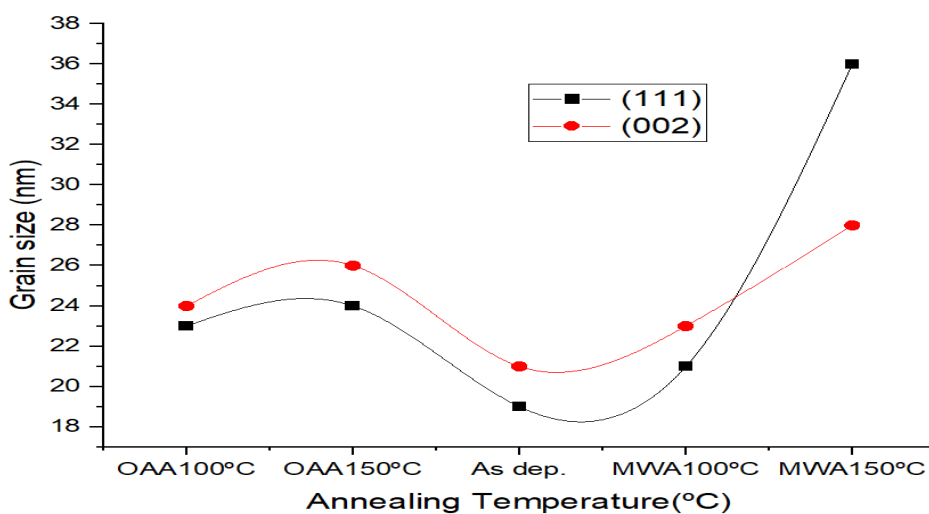


Figure 4: The Grain size of the ZnO films.

The FWHM of the diffraction peak of the (002) and (111) direction is plotted in Figure 5. It can be seen that the intensity of the ZnO thin film increases as the annealing temperature

increases indicating that the FWHM is strongly related to the intrinsic defects, such as oxygen vacancies, and the antisite defect.

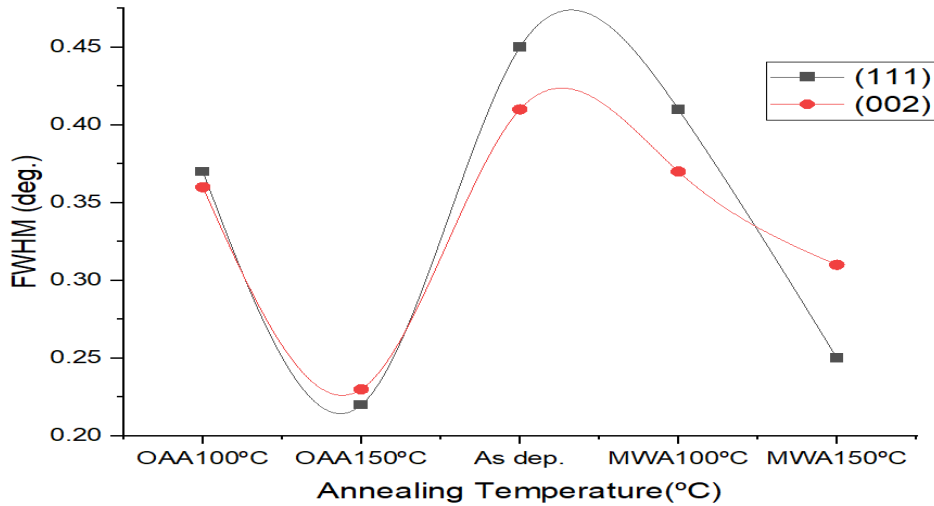


Figure 5: The FWHM of the (111) and (002) diffraction peaks

Optical properties

Figure 6 shows the optical transmittance of the samples' ZnO thin films. All the films show high optical transmittance in the visible region of the electromagnetic spectrum. The annealed films have higher transmittance than the as-deposited sample. The absorption edge at $\lambda = 350$ nm for all the samples is due to absorption of the glass substrate (Kazee m et al., 2021).

ZnO thin films have this maximum at $\lambda = 650$ nm while for minimum value depends on the film's thickness. Moreover, the location of this minimum is associated with the film thickness and disappears at the deposition of the film. Thus, two different types of anomalies As-deposited and annealed inherent in ZnO films depending on the power and the least variable associated with the thickness of the film.

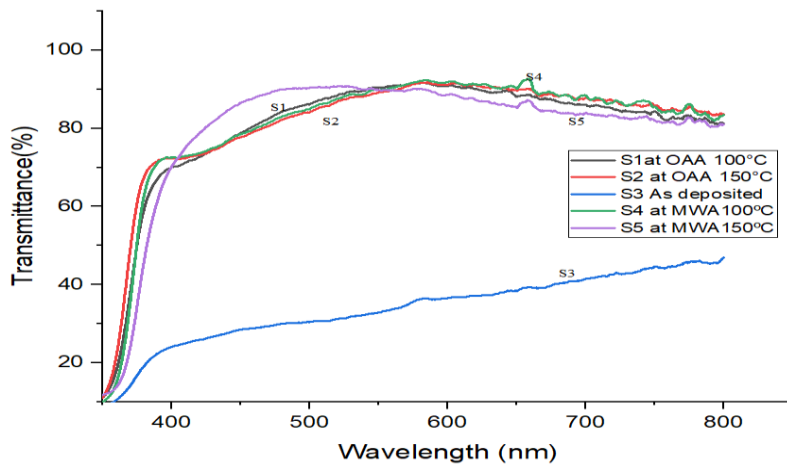


Figure 6: Optical transmittance of ZnO films

The optical reflectance spectrum of the ZnO films is shown in Figure 7. All the films show low optical reflectance in the visible region of the electromagnetic spectrum. The annealed films have a lower reflectance than the as-deposited films. The reflectance of the as-deposited (S_3), samples S_1 , S_2 , S_4

and S_5 are 14.55%, 26.86%, 28.22%, 27.09% and 23.78% respectively. The high transmittance and low reflectance properties of the films make them good materials for anti-reflection coatings and for solar thermal applications in flat plate collectors. (Moreh et al., 2014).

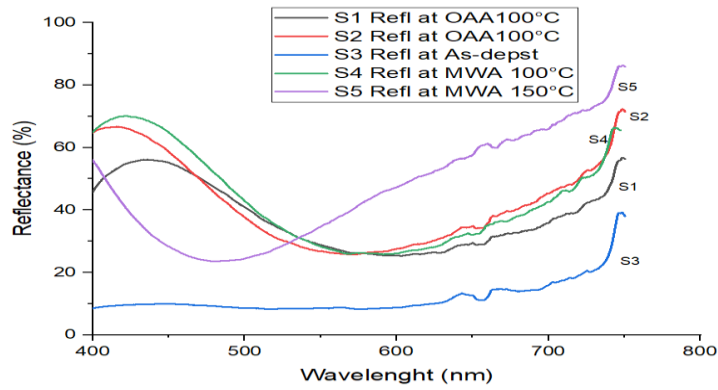


Figure 7: Optical reflectance of ZnO films versus wavelength.

The ability of a material to absorb light is measured by its absorption coefficient. Figure 8 shows the variation of the absorption coefficient of ZnO films with various wavelength regions annealed at different temperatures. It can be seen that sample S₃ has a higher absorption coefficient than the annealed films. This implies that the as-deposited films have higher ability to absorb light within the visible region than the

other samples annealed at different temperatures. The absorption coefficient of the ZnO films is shown in Table 3. According to (Balu et al., 2014), this higher value of α for as-deposited ZnO films with steeper optical absorption edge indicates better crystallinity of the films and lower defect density near the band edge.

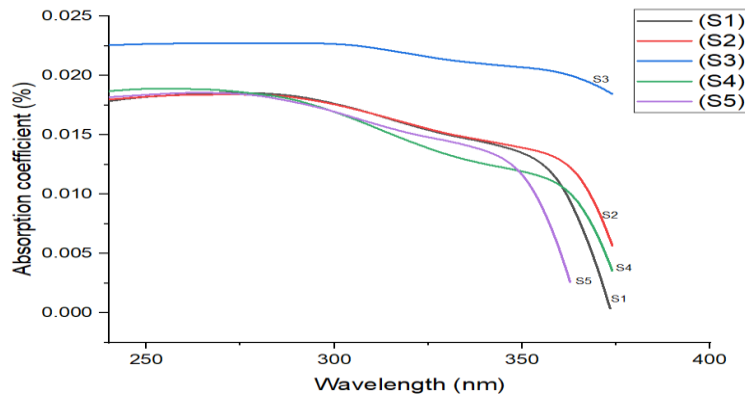


Figure 8: Variation of absorption coefficient with wavelength.

Table 2: Absorption coefficient of ZnO films annealed at different temperatures

SAMPLES	ABSORPTION COEFFICIENT, $\alpha(\text{CM}^{-1})$
As deposited	0.0225
ZnO film annealed at 100°C OAA	0.0179
ZnO film annealed at 150°C OAA	0.0180
ZnO film annealed at 150°C OAA	0.0186
ZnO film annealed at 150°C OAA	0.0181

The optical band gap of the ZnO thin films was calculated from the allowed direct transition for Equation (5). The optical bandgaps (E_g) of all the samples are listed in Table 3. It can be seen that the bandgap (E_g) increases with an increase in annealing temperature. It is generally believed that this increase in the band gap is due to the Burstein-Moss shift that

is due to increase in carrier concentration, and the absorption edge shifts to a higher energy level. (Abdullahi et al., 2015). Figure (9a) shows the extrapolated energy band gap for the as-deposited sample. The band gap was determined at 2.96 eV, which is less than that of ZnO, as reported by other researchers (Yu-Hsiu, 2009.; Gadallah and El-Nahass, 2013). The decrease may be attributed to the quantum size effect.

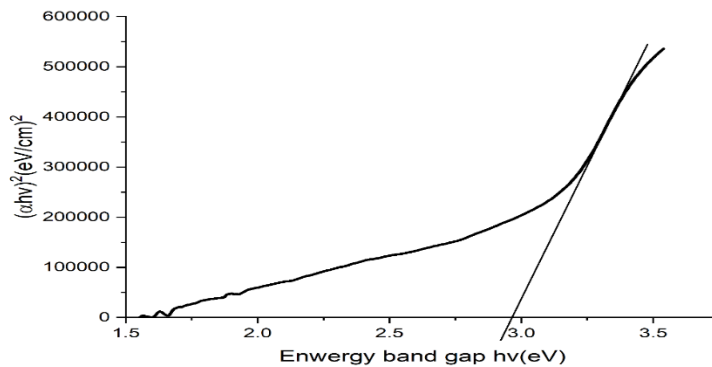


Figure 9a: A plot of $(\alpha hv)^2$ against $h\nu$ for As-deposited sample

Figure (9b) is the band gap of sample (S₁) annealed in open air at 100°C, the band gap is 3.29 eV. Many literatures have shown that the band gap of ZnO is between (3.3-3.4 eV). Therefore, for this sample, there is also a decrease which may

be due to reducing the density of dangling bonds, redistributing atomic distances and bond angles and the optical gap then increases.

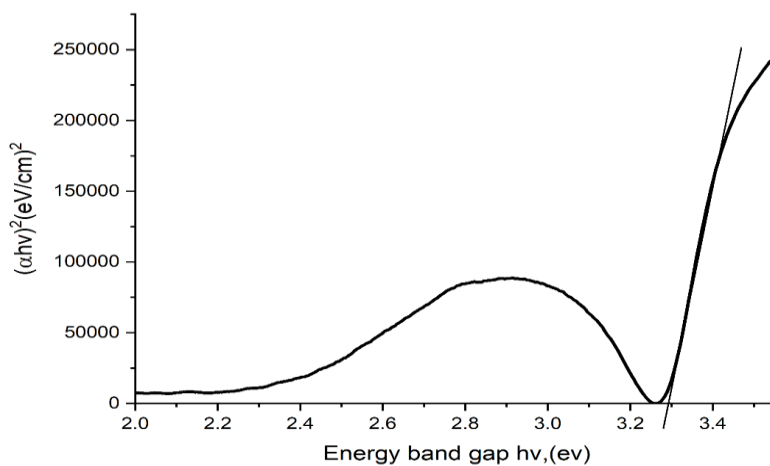


Figure 9b: A plot of $(\alpha hv)^2$ against $h\nu$ for ZnO annealed at 100°C in open air

Figure 9c belongs to the ZnO sample (S₂) annealed in open air at 150°C. The band gap stood at 3.32 eV, indicating that the band gap sample showed good transmission. Increase in the

band gap is due to the Burstein-Moss shift which is due to an increase in carrier concentration and the absorption edge shifts a higher energy level.

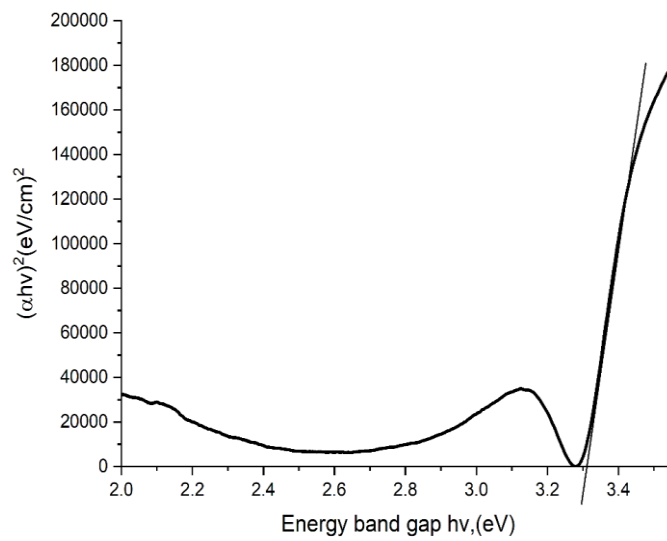


Figure 9c: A plot of $(\alpha hv)^2$ against hv for ZnO annealed at 150°C in open air

The band gap of sample (S4) is shown in Figure (9d) the band gap is 3.29 eV having the same optical bandgap as sample (S1).

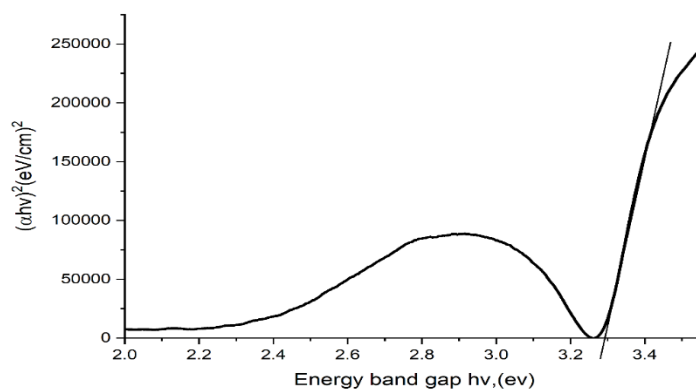


Figure 9d: A plot of $(\alpha hv)^2$ against hv for ZnO annealed at 100°C in microwave

Figure 9e belongs to the ZnO sample S5. The band gap is 3.34 eV, this shows that there is an increase in the band gap which may be due to an increase in carrier concentration, the absorption edge shifting to a higher energy level.

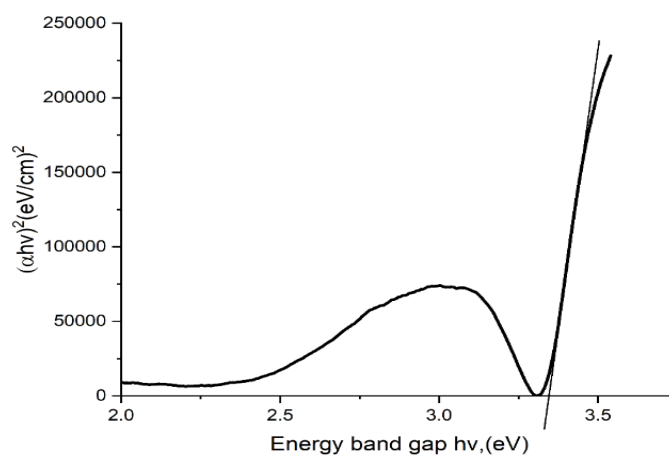


Figure 9e: A plot of $(\alpha hv)^2$ against hv for ZnO annealed at 150°C in microwave

Table 3: Energy band gap ZnO thin films

S/NO	SAMPLES	ENERGY BAND GAP Eg. (eV)
1.	As-deposited	2.96ev
2.	Annealed at 100°C for OAA	3.29ev
3.	Annealed at 150°C for OAA	3.32ev
4.	Annealed at 100°C for MWA	3.29ev
5.	Annealed at 150°C for MWA	3.34ev

CONCLUSION

The effect of open-air annealing (OAA) and microwave annealing (MWA) on the structural and optical properties was investigated. The results obtained indicate that the optical and structural properties depend strongly on the considered lower annealing temperature. The annealing temperatures employed in this research considerably decrease the production/growth duration to a minimum of 30 minutes for OAA and a maximum of 60 minutes for MWA compared to previous reports (Khan et al, 2021, Abdullahi et al, 2017 and Moreh et al, 2014). The optical and structural properties analysis showed that the annealing temperature considered had significantly improved the optical and structural properties of the deposited thin films presented in this work and the following findings are summarized:

REFERENCES

Abdullahi, S., & Maiyama, B. A. (2017). The Role of Air Annealing on the Structural and Electrical Properties of Zinc Oxide (ZnO) Thin Film Deposited by Rf Sputtering Technique: Scholars. *Journal of Engineering and Technology*, 5(12), 704-708.

Abdullahi, S., Momoh, M., Moreh, A.U., Isah, K.U., & Argungu, G.M. (2015). Influence of Thickness on Optical Properties of ZnO Thin Films prepared by Radio Frequency Sputtering Technique. *Nigerian Journal of Solar Energy*, 26, 66-70.

Abdullahi, S., Momoh, M., Moreh, A.U., Bayawa, A. M., Hamza, B., Argungu, G.M., & Popoola, O. T. (2017). Influence of Annealing Temperature on Optical and Electrical Properties of Cu₂ZnSnS₄(CZTS) thin Films Deposited by Sputtering Method from a Single Quaternary Target. *International Journal of Scientific Research in Science and Technology*, 3(1), 77-82.

Abdullahi, S., Momoh, M., & Isah, K. U. (2014). Electrical and Structural Properties of Radio Frequency (RF) Sputtered ZnO Thin Film at Low Substrate Temperature. *Journal of Electrical Engineering*, vol 2, pp 12-19.

Al-ofin, H. H., Abdel-Raheem, M. M., Ateyyah., & Al-Baradi, M. (2012). Structural and optical properties of Al₂ZnO₄ thin films deposited by D.C. sputtering technique. *Journal of non-oxide Glasses*, 3(3), pp39 – 54.

Balu, A. R., Manyula, N., Usharani, K., Nagarethinam, V. S. (2014). Studies on the Physical Properties of three potentially important TCO Thin Films fabricated by a Simplified Spray Technique under same Deposition conditions. *International Journal of chem Tech Research*, 6(1), 34-38.

Chaitra, U., Kekuda, D., & Rao, K.M. (2017). Effect of annealing temperature on the evolution of structural, microstructural, and optical properties of spin coated ZnO thin films. *Ceramics International*, 43(9), No.71, pp15-22.

Davidse, P. D., and Maissel, L. I. (1966). Dielectric Thin Films through rf Sputtering. *Journal of Applied Physics*, 37, 574. <https://doi.org/10.1063/1.1708218>.

Eya, D.D.O. (2006). Optical properties and applications of cadmium selenide (CdSe) thin films prepared by chemical bath deposition technique, *The Pacific Journal of Science and Technology*, Vol. 7, No. 1, pp 64–68.

Gadallah, A., & El-Nahass, M. M. (2013). Structural, Optical Constants and Photoluminescence of ZnO Thin Films Grown by Sol-Gel Spin Coating. *Advances in Condensed Matter Physics*, 1- 11. <http://dx.doi.org/10.1155/2013/234546>

Godbole, B., Badera, N., Shrivastava, S., Jain, D. & Ganesan, V. (2011). Growth mechanism of ZnO films deposited by spray pyrolysis technique. *Materials Science and Applications*, Vol. 2, No. 6, pp.643–648.

Gonçalves, R. S., Petrucio, B., & Cunha, F. (2016). Optical and structural properties of ZnO thin films grown by magnetron sputtering: effect of the radio frequency power. *Thin Solid Films*, (616), 265-269.

Kazeem, A. M., Akintunde, A. A., Aderemi, B. A., & Olutayo, W. A. (2021). Structural and optical characterization of chemically synthesized nanostructure zinc oxide thin film: ABU Ainternational. *journal of natural and applied science*,1(1),18-2. <https://doi.org/10.53982/ajnas.2021.0101.03-j>

Kumar, G.A., Reddy, M.R., & Reddy, K. N. (2015). Structural and Optical properties of ZnO thin films grown on various substrates by RF magnetron sputtering. In IOP Conference Series: IOP Publishing. *Materials Science and Engineering* Vol. 73, No. 1, p. 012-133.

Laurenti, & Cauda, P. (2018). Zinc Oxide Thin Films: Synthesis Approaches and Applications. *Coatings* 2018, 8(2), 67. <https://doi.org/10.3390/coatings8020067>

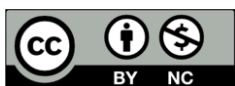
Moreh, A. U., Momoh, M., Hamza, B., Abdullahi, S., Yahya, H. N., Namadi, S., & Umar, S. (2014). Influence of substrate temperature on electrical resistivity and surface morphology of CuAlS₂ thin films prepared by thermal evaporation method, *Int. J. Nano Ma ter. Sci.* 3, pp 47- 55.

Pankaj, K., Bhujbal, H. M., Pathan, N., & Chaure, B. (2020). Temperature Dependent Studies on Radio Frequency Sputtered Al Doped ZnO Thin Films, *Engineered Science*, 10, 58–67. <https://dx.doi.org/10.30919/es8d1003>

Raghavendra, P. V., & Bhat, J. S. (2017). Optical properties of strontium doped zinc oxide thin films: AIP Conference Proceeding <https://doi.org/10.1063/1.4980527>

Senay, V., Pat, S., Korkmaz, S., Aydoğmus, T., Elmas, S., Özen, S., Ekem, N., Balbağ, M.Z. (2014). ZnO thin film

- synthesis by reactive radio frequency magnetron sputtering. *Applied Surface Science*. No.1, vol.318, pp.2-5.
- Shakoury, R., Arman, A., & Miri, S. (2022). Optical properties and microstructure of ZrO₂ thin films deposited by RF magnetron sputtering: case study on effects of different working temperatures. *Opt Quant Electron* 54, 682
- <https://doi.org/10.1007/s11082-022-04071-2>
- Shun-Fa, H., Li, W. (2013). PZT Thin Films Deposited by RF Magnetron Sputtering. *Applied Mechanics and Materials*. 302, 8-13.
- Tchenka, A., Agdad, A., Samba, M. C., Hnawi, S. K., Narjis, A., Nkhaili, L., Ibnouelghazi, E. & Ech-Chamikh, E. (2021). Effect of RF Sputtering Power and Deposition Time on Optical and Electrical Properties of Indium Tin Oxide Thin Film. Volume 2, <https://doi.org/10.1155/2021/5556305>
- Yilmaz, M. (2014). Characteristic properties of spin coated ZnO thin films: the effect of Ni doping, *The Royal Swedish Academy of Sciences. Physica Scripta*, Volume 89, Number 9. DOI 10.1088/0031-8949/89/9/095802
- Yu-Hsiu, L. (2009). Structure and properties of transparent conductive ZnO films grown by pulsed laser deposition (PLD) *Doctoral dissertation University of Birmingham, United Kingdom, 2009.*
- Viswanathan. K., Shyju, T.S., Ramachandran, D., & Pradhaban, G. (2016). Electric properties of ZnO thin films by RF Magnetron sputtering technique: *Proceedings. Materials Today* 3(6),15,48-52.
- Vyas, S. (2020). A Short Review on Properties and Applications of Zinc Oxide Based Thin Films and Devices. *Johnson Matthey Technol. Rev*, 64(2), 202. doi: 10.1595/205651320X15694993568524
- Zulkifli, Z., Sharma, S., Shinde, S., Kalita, G., Tanemura, M. (2015). Effect of annealing in hydrogen atmosphere on ZnO films for field emission display. *INOP Conference Series: Materials Science and Engineering* Vol. 99, No. 1, p. 012-030).



©2023 This is an Open Access article distributed under the terms of the Creative Commons Attribution 4.0 International license viewed via <https://creativecommons.org/licenses/by/4.0/> which permits unrestricted use, distribution, and reproduction in any medium, provided the original work is cited appropriately.